CrossMark

ORIGINAL PAPER

Dynamic Fracture Properties of Rocks Subjected to Static Pre-load Using Notched Semi-circular Bend Method

Rong Chen[1] · Kang Li[1] · Kaiwen Xia[2] · Yuliang Lin[1] · Wei Yao[2] · Fangyun Lu[1]

Abstract   A dynamic load superposed on a static pre-load is a key problem in deep underground rock engineering projects. Based on a modified split Hopkinson pressure bar test system, the notched semi-circular bend (NSCB) method is selected to investigate the fracture initiation toughness of rocks subjected to pre-load. In this study, a two-dimensional ANSYS finite element simulation model is developed to calculate the dimensionless stress intensity factor. Three groups of NSCB specimen are tested under a pre-load of 0, 37 and 74 % of the maximum static load and with the loading rate ranging from 0 to 60 GPa m$^{1/2}$ s^{-1}. The results show that under a given pre-load, the fracture initiation toughness of rock increases with the loading rate, resembling the typical rate dependence of materials. Furthermore, the dynamic rock fracture toughness decreases with the static pre-load at a given loading rate. The total fracture toughness, defined as the sum of the dynamic fracture toughness and initial stress intensity factor calculated from the pre-load, increases with the pre-load at a given loading rate. An empirical equation is used to represent the effect of loading rate and pre-load force, and the results show that this equation can depict the trend of the experimental data.

✉ Kaiwen Xia
 kaiwen@ecf.utoronto.ca

1   College of Science, National University of Defense Technology, Changsha 410073, Hunan, People's Republic of China

2   Department of Civil Engineering and Lassonde Institute, University of Toronto, Toronto, ON M5S 1A4, Canada

List of symbols

BD	Brazilian disc
ISRM	International Society for Rock Mechanics
CCNSCB	Cracked chevron notched semi-circular bend
NSCB	Notched semi-circular bend
SHPB	Split Hopkinson pressure bar
a	The length of the notched crack of the NSCB specimen
A_0	The cross-sectional area of the bar
B	The thickness of NSCB and CCNSCB specimen
E_0	The Young's modulus of the bar material
f_D	The scale factor of dynamic fracture toughness over the static fracture toughness
f_{Dp}	The scale factor of dynamic fracture toughness with pre-load over the static fracture toughness
K_I	The stress intensity factor for mode-I fracture in NSCB specimen
K_{Ic}	The quasi-static fracture toughness
K_{Id}	The dynamic fracture toughness
K_{I_total}	The total fracture toughness
K_{I_pre}	The stress intensity factor due to the pre-load
P_1	The forces at the incident end of the specimen
P_2	The transmitted end of the specimen
$P_{dynamic}$	The dynamic load
P_{max}	The maximum value of the load
P_{pre}	The pre-load
P_{total}	The total load
$P(t)$	The time-varying loading force
R	The radius of NSCB specimen
R_S	The radius of diamond-impregnated blade saw
S	The span of the supporting pins
$Y(a/R)$	The dimensionless stress intensity factor
ε_i	The incident stress wave

ε_r The reflected stress wave
ε_t The transmitted stress wave

1 Introduction

In the past few decades, the mechanical response of rocks under static and dynamic loading has been studied extensively and significant progress has been made in the characterization of dynamic properties of rocks (Dai et al. 2010; Xia et al. 2008; Xia and Yao 2015). Testing methods and techniques for dynamic compressive strength (Xia et al. 2008), dynamic tensile strength (Huang et al. 2010), dynamic flexural strength (Dai et al. 2013) and dynamic fracture toughness (Chen et al. 2009; Dai and Xia 2013; Zhang and Zhao 2014) have been developed and improved. In these tests, rock specimens are stress free before being subjected to dynamic loading. Due to the importance of dynamic mechanical properties of rocks, the International Society for Rock Mechanics (ISRM) Commission on Rock Dynamics published suggested methods for determining dynamic strength parameters and mode-I fracture toughness of rock materials (Zhou et al. 2012).

With the further development of the mining industry and the increasing depth of underground engineering, rock is often subjected to dynamic impact under pre-load. For example, in underground mining processes, tectonic stress and gravity are typical static pre-loads which act on underground rock engineering structures. In addition, these structures may also be exposed to dynamic loads due to production blasting nearby or rock bursts or earthquakes. Under these circumstances, the dynamic response of rock subjected to static pre-load is crucial to the safety of workers, equipment and engineering facilities.

There are also many unique phenomena observed in underground engineering activities that cannot be explained by means of existing rock mechanics theories. Especially for rocks at depths of 1000 m and more below the ground surface, abnormal phenomena (e.g., rockburst, zonal disintegration, core discing) become more prominent, leading to an enormous challenge to the traditional rock mechanics (Qian 2004; Zhou et al. 2005). Traditional fracture criteria and strength theories are not applicable when the rocks are under the dynamic load superimposed with static pre-load, because the measured total rock strength is different from the summation of the rock dynamic strength and the static pre-load (Li et al. 2008b). Therefore, it is necessary to investigate the dynamic properties of rocks subjected to static pre-load.

Since 2002, there have been many investigations on the issue of rock strength for rocks subjected to the dynamic load superposed with static pre-load (Gong et al. 2010; Li et al. 2008a, b; Zhou et al. 2014). Based on the modified split Hopkinson pressure bar system, Li et al. (2008a) proposed an innovative testing technique for dynamic compressive tests of rock subjected to static pre-load. Tests on siltstone specimens with different pre-loads under different loading rates indicated that the total compressive strength of the specimen under simultaneous static pre-load and dynamic load was higher than the sum of its dynamic compressive strength at the same loading rate and the pre-load (Li et al. 2008a). The strength of rock under superposed loads (dynamic load plus the static pre-load) decreases rapidly when the axial pre-compression stress is greater than 70 % of the static strength of rock (with identical impact loading). Even though the far-field load is compressive, the local stresses may be tensile. For example, the roof of an underground opening will undergo in situ tensile stresses because of the roof bending. Therefore, it is necessary to investigate the dynamic tensile failure of rock materials under pre-tension. Dynamic Brazilian disc (BD) tests on granite under pre-tension were conducted by Zhou et al. (2014). The test results showed that the tensile strength of the granite decreased with increasing static pre-stresses, which might lead to modifications of the blasting design or support design in deep underground projects. Using similar methods, Wu et al. (2015) showed that although the dynamic tensile strength decreased with the pre-stress, the total strength (the sum of the dynamic tensile strength and the static pre-tension stress) was approximately independent of the pre-stress. Both the dynamic strength and the total strength increase with the loading rate as shown in the two studies mentioned above.

Despite recent efforts and results on the effect of pre-load on the dynamic mechanical responses of rocks, the influence of pre-load on the dynamic fracture properties and the crack propagation process remains unknown. It is thus the objective of this paper to fill in this gap. In this paper, a modified split Hopkinson pressure bar (SHPB) test system was used to carry out dynamic tests on the rock specimens under pre-stress conditions. The notched semi-circular bend (NSCB) specimens were selected to investigate the fracture initiation toughness or simply fracture toughness. The NSCB method was used to study the dynamic fracture initiation toughness and some other fracture parameters by Chen et al. (2009) and Xia et al. (2013). This method has been verified by Dai et al. (2010). In material dynamic tests, it is desirable to ensure the dynamic force balance of the specimen. For example, in dynamic compressive tests, the dynamic force balance guarantees the uniformity of the specimen and thus the calculated rock strength is valid. The same is true for other dynamic rock tests. Theoretically, the time needed for a

specimen to reach the dynamic force balance is equal to three times the traveling time of the stress wave through the specimen. Thus, a short specimen is favored in dynamic tests. The length of the NSCB specimen is half of that of a full disc specimen. Further as compared with the traditional three-point bending specimen, one only needs to align the two supporting points on the transmitted bar side, thus facilitating specimen alignment. The NSCB method was therefore chosen as the ISRM-suggested method for quantification of rock dynamic fracture toughness (Zhou et al. 2012).

This paper is organized as follows. After the introduction, Sect. 2 introduces the specimen preparation and experimental setup. Measurement principles are detailed in Sect. 3 and the results are presented in Sect. 4, along with a discussion. Section 5 summarizes the entire paper.

2 Specimen Preparation and Methodology

2.1 Specimen Preparation

The specimen is made from Heshuo granite in the Northeast region of Heshuo, Xinjiang Province, China. It consists of 25 % quartz, 10 % common feldspar, 63 % plagioclase and the remaining 2 % biotite. The typical micrographs of the granite were obtained from thin sections using polarized light and illustrated in Fig. 1.

Figure 2 shows the schematic of an NSCB specimen in the SHPB system. The specimen radius R is 24 mm, the thickness B is 18 mm, the length of the notched crack a is 4 mm and the span of the supporting pins S is 30 mm. The outer diameter of the adapter is 10 mm and the inner diameter is 20.1 mm; the diameter of the support pin is 6 mm.

Rock specimens were cored with a nominal diameter of 48 mm and then sliced into disc specimens with a thickness of 18 mm. By diametrical cutting, half disc specimens
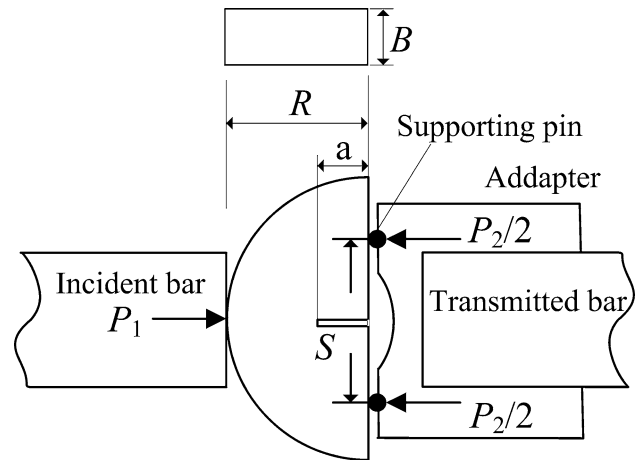

Fig. 2 The schematic of the NSCB specimen in the SHPB system

were subsequently made from the full discs. As has been discussed by Lim et al. (1994), a pre-crack at the tip of the notch may not be necessary for some rocks if the notch is sufficiently small (<0.8 mm); thus the NSCB specimens in this study were prepared with a 1 mm-wide notch firstly and then sharpened at the tip by a diamond wire saw to achieve a tip width of 0.5 mm. The average grain size of the granite in this study is about 1 mm, which is larger than the width of the notch tip. Therefore, the specimens are suitable for the fracture toughness tests.

2.2 Test Apparatus and Scheme

To simulate the dynamic loading conditions superposed on a static pre-load, the traditional SHPB device was modified. Figure 3 shows the modified system for the dynamic test under static pre-load based on the SHPB test platform. The entire system consists of an axial compressive loading unit and a traditional SHPB test platform. The axial compressive unit is connected to the hydraulic control system through the high-pressure pipeline. The hydraulic
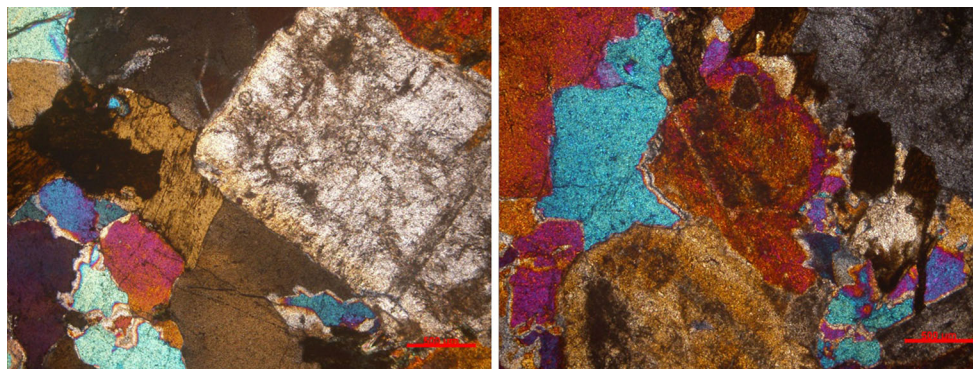
Fig. 1 Micrographs of Heshuo granite with polarized light

Fig. 3 Configuration of the loading system for dynamic tests under pre-load (pulse shaper made of black rubber sheet is shown on the impact end of the incident bar)
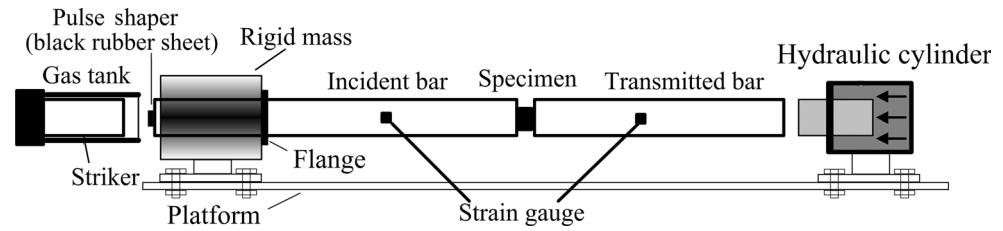
confinement is computer controlled, so that the pre-stress can be controlled.

The parameters of the modified SHPB are summarized in Table 1. At the beginning of the experiment, the rigid mass and the hydraulic cylinder were fixed on the supporting platform (as shown in Fig. 3), and the hydraulic cylinder was then pressurized to the desired value. The pressure was transmitted to the bar systems, because the rigid mass constrains the leftward axial motion of the bars through a flange attached to the incident bar (Fig. 3). However, the motion of the bars associated with impact is rightward and thus the flange does not affect stress wave propagation. When the axial pressure reached the desired value, the striker bar was launched to apply dynamic loading by the impact on the free end of the incident bar. The incident pulse propagates along the incident bar before it hits the specimen, leading to a reflected stress wave and a transmitted stress wave that are recorded by the strain gauges attached on the incident and transmitted bar surfaces. Denoting the incident wave, the reflected wave and the transmitted wave by ε_i, ε_r and ε_t, respectively, and assuming one-dimensional stress wave propagation in the bar and specimen and stress equilibrium in the specimen during loading ($P_1(t) = P_2(t)$), the time-varying dynamic forces on both ends of the specimen can be determined as (Zhou et al. 2012):

$$P_1(t) = A_0 E_0 [\varepsilon_i(t) + \varepsilon_r(t)] + A_0 \sigma_0, \\ P_2(t) = A_0 E_0 \varepsilon_t(t) + A_0 \sigma_0, \tag{1}$$

where A_0 is the cross-sectional area, E_0 is the Young's modulus of the bar and σ_0 is the pressure of the hydraulic oil. It is noted that if the oscilloscope channels for the strain gauge were set to AC coupling, only the change of the stress could be measured, and static pre-load $A_0 \sigma_0$ is not recorded in the signal from the strain gauges during the dynamic tests. In our test, the oscilloscope channels are set to AC coupling; thus the force balance condition ($P_1(t) = P_2(t)$) should be written as:

$$A_0 E_0 [\varepsilon_i(t) + \varepsilon_r(t)] = A_0 E_0 \varepsilon_t(t). \tag{2}$$

3 Measurement Principles

Under the condition that the specimen is in a state of dynamic force balance during the test, the specimen has achieved a quasi-static state (Dai et al. 2010). Therefore, the fracture properties can be deduced via a quasi-static method based on linear elastic fracture mechanics. According to the ASTM standard E399-06e2 for a rectangular three-point bending specimen, the stress intensity factor for mode-I fracture in the NSCB specimen can be determined as:

$$K_I(t) = \frac{P(t)S}{BR^{3/2}} Y\left(\frac{a}{R}\right), \tag{3}$$

where S is the span of the supporting pins; $P(t)$ is the time-varying loading force in the specimen, which is $P_1(t)$ ($=P_2(t)$) and can be calculated from the transmitted signal referred to the study conducted by Chen et al. (2010). $Y(a/R)$ is the dimensionless stress intensity factor and calculated via numerical methods as detailed below.

ANSYS finite element analysis software is applied for the numerical calculation of $Y(a/R)$. Since the crack is straight in the NSCB, the half-crack model is used to calculate the dimensionless stress intensity factor. The PLANE82 (eight-node) element in ANSYS is implemented to build this model, and the quarter-point element is applied near the crack tip to simulate the stress field more precisely. The elastic modulus and Poisson's ratio in the FEM analysis are 50 GPa and 0.21, respectively. There are totally 1998 elements and 6111 nodes, as shown in the finite element model schematic of Fig. 4. Due to the fact that the lower side of the model is a symmetric plane, the symmetry constraint is imposed on this surface, and the

**Table 1** Summary of the parameters in the modified SHPB

Diameter of bars (mm)	Striker bar length (mm)	Incident bar length (mm)	Transmitted bar length (mm)	Young's modulus (GPa)	Density (kg/m³)
20	200	2000	1200	71	2700
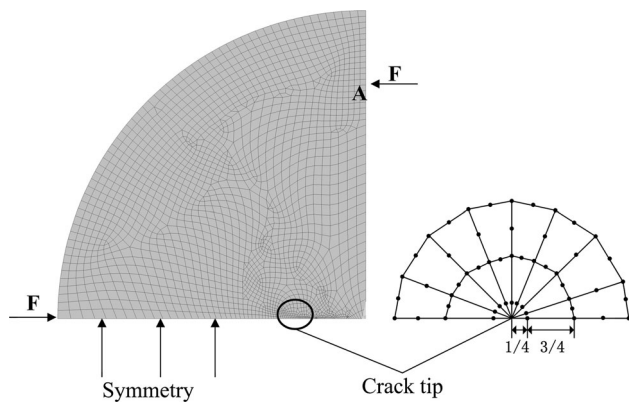
Fig. 4 Schematic of the NSCB specimen's finite element model with quarter-point element on the crack tip
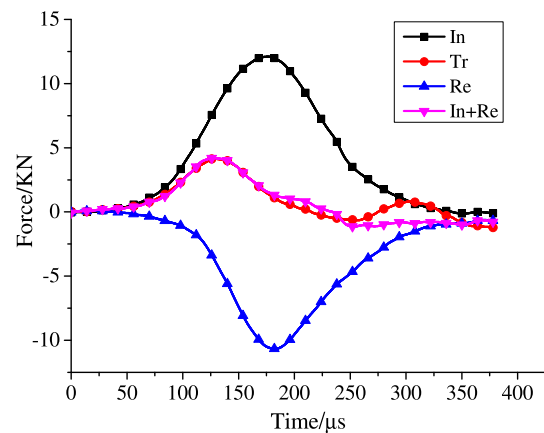
Fig. 6 Dynamic force balance in a typical NSCB–SHPB test with pulse shaping
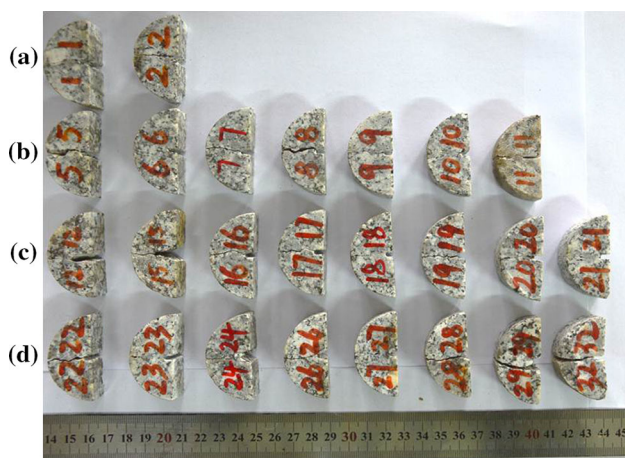
Fig. 5 Photograph of recovered specimens: **a** quasi-static experiment, **b** dynamic experiment without pre-load, **c** dynamic experiment with 37 % of the static critical load as pre-load and **d** dynamic experiment with 74 % of the static critical load as pre-load

length of the symmetry constraint is 24 mm. The forces applied on both sides of the specimen during the dynamic test are identical; thus the force F is taken as the half of the loading force P_1 or P_2. The fracture toughness K_{Id} is that for the maximum value of the loading force P_{max}. Furthermore, $Y(a/R)$ is determined from K_{Id} and P_{max} as:

$$Y\left(\frac{a}{R}\right) = \frac{BR^{3/2}}{SP_{max}(t)}K_{Id}(t). \tag{4}$$

4 Results and Discussion

Tests were conducted on approximately 36 rock specimens, and 22 tests yielded valid strain data. Figure 5 shows the recovered specimens; all the specimens were broken from the notch tip.
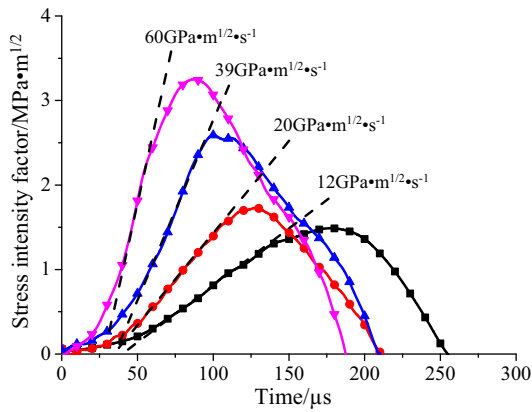
4.1 Stress Equilibrium

To use Eq. (3) to calculate the fracture toughness, the pulse shaper technique was applied to achieve the dynamic force balance in the specimen during the experiments. Referring to the discussion by Frew et al. (2002) on details for SHPB compressive tests for brittle materials, a 4 mm × 4 mm square black rubber sheet with 1 mm thickness was used as a pulse shaper, which was placed at the free end of the incident bar (Fig. 3). The pulse shaper reduces the rising slope of the incident pulse and shapes the incident wave from rectangular to ramped.

Figure 6 shows the forces on both ends of the NSCB specimen in a typical dynamic test under pre-load, which was set at 37 % of the static critical load. The dynamic force is balanced, which is the same as the traditional SHPB test. The dynamic stress on one side of the specimen is the sum of the incident and reflected stress waves (P_1), and the dynamic stress on the other side of the specimen is the transmitted stress wave (P_2). As shown in Fig. 6, the forces on both ends of the specimen P_1 (=In + Re) and P_2 (=Tr) are in good agreement before 180 μs (i.e., P_1 is equal to P_2). This eliminates the global force difference and thus the inertial effects are negligible (Weerasooriya et al. 2006). Therefore, the specimen is in dynamic stress equilibrium before fracture, and the quasi-static method is reasonable for data analysis.

4.2 Effects of Loading Rate

The loading rate is defined as the rate of change of the stress intensity factor at the crack tip with time according to the dynamic fracture toughness method suggested by ISRM (Zhou et al. 2012). Figure 7 shows four typical NSCB test results regarding stress intensity factor with different loading rates. There exists an approximately

Fig. 7 Stress intensity factor versus time curves for different loading rates in NSCB tests

Fig. 8 Normalized dynamic crack initiation toughness as a function of normalized loading rate for several rocks

linear region in $K_I(t)$, and its slope is taken as the loading rate. For example, in the curve with the maximum fracture toughness of 2.55 MPa m$^{1/2}$, the region between 56.5 and 87.5 μs is approximately linear. Thus, the slope of this region is chosen as the loading rate for this test. The loading rates are 12, 20, 39 and 60 GPa m$^{1/2}$ s^{-1}, and the corresponding fracture toughnesses (i.e., the maximum of the curves) are 1.46, 1.72, 2.55 and 3.26 MPa m$^{1/2}$, respectively. The results indicate that the fracture toughness increases with the increasing loading rate, revealing the phenomenon of rate dependency that is shared with other mechanical properties (e.g., compressive and tensile strength) of the rock material (Zhang et al. 1999).

In this work, we normalized both the dynamic crack initiation toughness and the loading rate with the quasi-static fracture toughness:
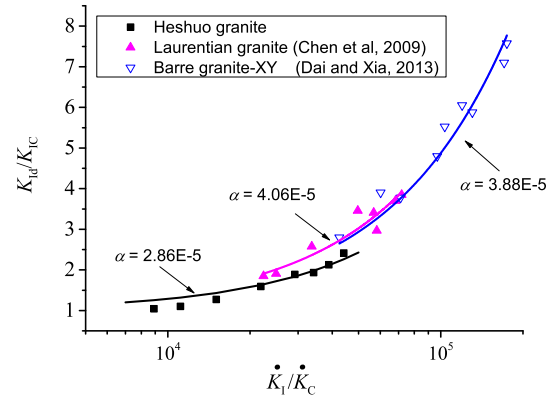
$$\frac{K_{Id}}{K_{IC}} = f_D\left(\frac{\dot{K}_I}{\dot{K}_C}\right), \tag{5}$$

where $f_D \geq 1$ is the function which takes into account the increased initiation toughness due to loading rates. K_{Id} is the dynamic fracture toughness, and K_{IC} is the quasi-static fracture toughness, which was measured in an MTS machine with the loading velocity of 2 mm/min using the same NSCB specimen geometry as the dynamic one. $\dot{K}_I$ is the loading rate, $\dot{K}_C \left(= \frac{\dot{K}_{IC}}{1s}\right)$ is the reference loading rate. Figure 8 shows the results of normalized dynamic crack initiation toughness as a function of normalized loading rate for Heshuo granite and two other granites. The latter were selected for comparison purposes.

Based on the results shown in Fig. 8, an empirical equation is proposed to fit the data and explain the dynamic behavior of at least for these three granites:

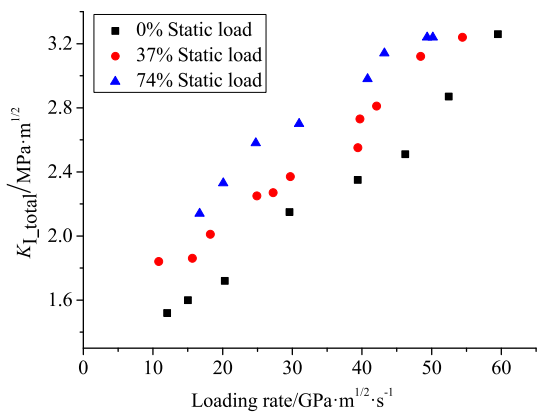$$f_D\left(\frac{\dot{K}_I}{\dot{K}_C}\right) = 1 + \alpha\left(\frac{\dot{K}_I}{\dot{K}_C}\right). \tag{6}$$

The second term represents the effect of loading rate dependence and the value of α is much smaller than 1. This means that when there is no dynamic loading, the value f_D is close to 1, and the initiation fracture toughness of the rock is quasi-static. The data fitting based on Eq. (4) and the data shown in Fig. 8 can be used to obtain the values of the parameters as: $\alpha = 2.86 \times 10^{-5}$, 4.06×10^{-5} and 3.88×10^{-5} for Heshuo granite, Laurentian granite and Barre granite-XY, respectively.

4.3 Effects of Loading Rate and Pre-load on Initial Fracture Toughness

As mentioned above, the fracture toughness measured with the NSCB method is actually the stress intensity factor when the crack begins to propagate, which is defined as the initiation toughness and reflects the ability of a material containing a crack to resist fracture initiation. Figures 9 and 10 show the dynamic test results of the NSCB specimens under three different pre-load conditions; the
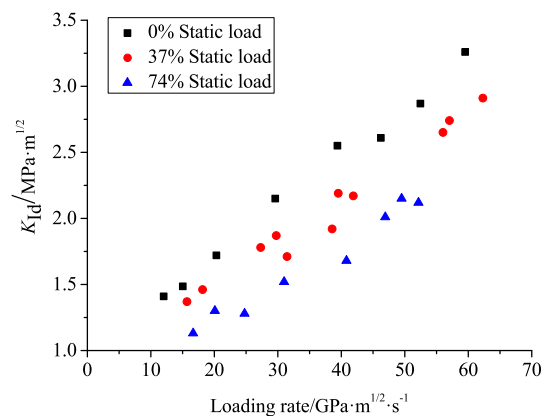
Fig. 9 The dynamic fracture toughness versus loading rate

Fig. 10 The total fracture toughness versus the loading rate

Fig. 11 Normalized dynamic crack initiation toughness as a function of normalized loading rate under different pre-loads

corresponding pre-loads in the NSCB specimen are 0, 37 and 74 % of the critical static load, which is a critical external load on the NSCB specimen when the fracture occurs under static loading.

Figure 9 illustrates the dynamic fracture toughness K_{Id} versus the loading rate under different pre-loads. In this case, the loading force P used in Eq. (3) for calculating K_{Id} is the dynamic force $P_{dynamic}$. The tendency of K_{Id} represents the dynamic loading capacity of a specimen under a certain static load which increases with the loading rate. It is observed that under the same loading rate, the initiation fracture toughness decreases with the pre-load. In other words, the specimen's dynamic impact load capacity is reduced by the pre-load, and the propagation of crack in the specimen can be initiated by a lower impact load.

Figure 10 shows the total fracture toughness K_{I_total} versus the loading rate. The loading force P used in Eq. (3) for calculating K_{I_total} is the sum of the pre-load and the dynamic force, i.e., $P_{total} = P_{dynamic} + P_{pre}$. Consequently, K_{I_total} indicates the total loading capacity under superposed loading conditions. Compared with the results shown in Fig. 9, Fig. 10 indicates that under the same dynamic loading rate, the total fracture toughness increases with the pre-load. It can also be seen that K_{I_total} is higher than K_{Id} under the same loading rate. Under the same loading rate, K_{Id} decreases with the increase of the pre-load, which means that pre-load weakens the rock material. However, K_{I_total} increases with the pre-load.

Similar to the empirical relation of dynamic fracture toughness, we normalize the dynamic fracture toughness with pre-load by K_{IC}:

$$\frac{K_{Id}}{K_{IC}} = f_{Dp}\left(\frac{\dot{K}_I}{\dot{K}_C}, \frac{K_{I\_pre}}{K_{IC}}\right). \tag{7}$$

In addition, two other terms are added to Eq. (6) to describe the effect of pre-load:
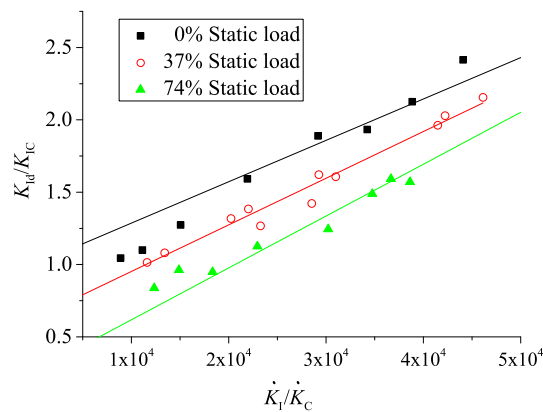
$$f_{Dp}\left(\frac{\dot{K}_I}{\dot{K}_C}, \frac{K_{I\_pre}}{K_{IC}}\right) = 1 - \frac{K_{I\_pre}}{K_{IC}} + \alpha\left(\frac{\dot{K}_I}{\dot{K}_C}\right) + \beta\left(\frac{\dot{K}_I}{\dot{K}_C}\right)\frac{K_{I\_pre}}{K_{IC}}, \tag{8}$$

where K_{I_pre} is the stress intensity factor due to the pre-load. When there is no stress intensity factor due to the pre-load ($K_{I\_pre} = 0$), Eq. (8) will degenerate to Eq. (6). When the specimen is loaded by the quasi-static condition ($\dot{K}_I \approx 0$), the parameter $f_{Dp} = 1 - K_{I\_pre}/K_{IC}$. For example, when the pre-load is 74 % of the critical static load, the specimen under quasi-static condition will be fractured when the additional quasi-static load is 26 % of the critical static load.

The experimental data fitting based on Eq. (7) results in the values of the parameters $\alpha = 2.86 \times 10^{-5}$ and $\beta = 9.78 \times 10^{-6}$. As shown in Fig. 11, the function fits well with the data points with the $r^2 = 97.8$ %, and the value is similar to the results obtained by Zhang and Zhao (2014) for Fangshan granite.

5 Conclusions

In this study, a modified SHPB test system was established to investigate the dynamic fracture behavior of rocks under a static pre-load. The NSCB method was applied to investigate the initiation fracture toughness. The numerical method based on ANSYS finite element analysis was used to calculate the dimensionless stress intensity factor of the NSCB specimens.

Experimental analyses indicate that the dynamic fracture toughness of rocks under pre-load is different from fracture toughness without pre-load. The test results demonstrate that the dynamic initiation fracture toughness decreases with the pre-load, implying that the dynamic load-bearing capacity of the engineering structure is relatively reduced under static

pre-load, which is of great significance to underground engineering design and assessment.

An empirical equation is used to simulate the effect of loading rate and pre-load force, and the results show that this equation fits well with the experimental data points.

References

Chen R, Xia K, Dai F, Lu F, Luo S (2009) Determination of dynamic fracture parameters using a semi-circular bend technique in split Hopkinson pressure bar testing. Eng Fract Mech 76:1268–1276. doi:10.1016/j.engfracmech.2009.02.001

Chen R, Guo X, Lu F, Xia K (2010) Research on dynamic fracture behaviors of stanstead granite. Chin J Rock Mech Eng 2:375–380

Dai F, Xia K (2013) Laboratory measurements of the rate dependence of the fracture toughness anisotropy of Barre granite. Int J Rock Mech Min 60:57–65. doi:10.1016/j.ijrmms.2012.12.035

Dai F, Chen R, Xia K (2010) A semi-circular bend technique for determining dynamic fracture toughness. Exp Mech 50:783–791. doi:10.1007/s11340-009-9273-2

Dai F, Xia K, Zuo JP, Zhang R, Xu NW (2013) Static and dynamic flexural strength anisotropy of Barre granite. Rock Mech Rock Eng 46:1589–1602. doi:10.1007/s00603-013-0390-y

Frew DJ, Forrestal MJ, Chen W (2002) Pulse shaping techniques for testing brittle materials with a split Hopkinson pressure bar. Exp Mech 42:93–106. doi:10.1007/BF02411056

Gong F, Li X, Liu X (2010) Experimental study of dynamic characteristics of sandstone under one-dimensional coupled static and dynamic loads. Chin J Rock Mech Eng 29:2076–2085

Huang S, Chen R, Xia KW (2010) Quantification of dynamic tensile parameters of rocks using a modified Kolsky tension bar apparatus. J Rock Mech Geotech Eng 2:162–168

Li X, Zhou Z, Lok T-S, Hong L, Yin T (2008a) Innovative testing technique of rock subjected to coupled static and dynamic loads.

Int J Rock Mech Min Sci 45:739–748. doi:10.1016/j.ijrmms.22007.08.013

Li X, Zhou Z, Ye Z, Ma C, Zhao F, Zuo Y, Hong L (2008b) Study of rock mechanical characteristics under coupled static and dynamic loads. Chin J Rock Mech Eng 27:1387–1396

Lim I, Johnston I, Choi S, Boland J (1994) Fracture testing of a soft rock with semi-circular specimens under three-point bending. Part 1—mode I. In: Int J Rock Mech Min Sci Geomech Abstr, vol 3, pp 185–197. doi:10.1016/0148-9062(94)90464-2

Qian Q (2004) The characteristic scientific phenomena of engineering response to deep rock mass and the implication of deepness. J East China Inst Technol 27:1–5

Weerasooriya T, Moy P, Casem D, Cheng M, Chen W (2006) A four-point bend technique to determine dynamic fracture toughness of ceramics. J Am Ceram Soc 89:990–995. doi:10.1111/j.1551-2916.2005.00896.x

Wu B, Chen R, Xia K (2015) Dynamic tensile failure of rocks under static pre-tension. In J Rock Mech Min Sci 80:12–18. doi:10.1016/j.ijrmms.2015.09.003

Xia K, Yao W (2015) Dynamic rock tests using split Hopkinson (Kolsky) bar system—a review. J Rock Mech Geotech Eng 7:27–59. doi:10.1016/j.jrmge.2014.07.008

Xia K, Nasseri MHB, Mohanty B, Lu F, Chen R, Luo SN (2008) Effects of microstructures on dynamic compression of Barre granite. Int J Rock Mech Min Sci 45:879–887. doi:10.1016/j.ijrmms.2007.09.013

Xia K, Huang S, Dai F (2013) Evaluation of the frictional effect in dynamic notched semi-circular bend tests. In J Rock Mech Min Sci 62:148–151. doi:10.1016/j.ijrmms.2013.06.001

Zhang Q, Zhao J (2014) A review of dynamic experimental techniques and mechanical behaviour of rock materials. Rock Mech Rock Eng 47:1411–1478. doi:10.1007/s00603-013-0463-y

Zhang Z, Kou S, Yu J, Yu Y, Jiang L, Lindqvist P-A (1999) Effects of loading rate on rock fracture. In J Rock Mech Min Sci 36:597–611. doi:10.1016/S0148-9062(99)00031-5

Zhou H, Xie H, Zuo J (2005) Developments in researches on mechanical behaviors of rocks under the condition of high ground pressure in the depths. Adv Mech 35:91–99

Zhou YX et al (2012) Suggested methods for determining the dynamic strength parameters and mode-I fracture toughness of rock materials. In J Rock Mech Min Sci 49:105–112. doi:10.1016/j.ijrmms.2011.10.004

Zhou Z, Li X, Zou Y, Jiang Y, Li G (2014) Dynamic Brazilian tests of granite under coupled static and dynamic loads. Rock Mech Rock Eng 47:495–505. doi:10.1007/s00603-013-0441-4